Applied Geochemistry 198 (2026) 106684

Contents lists available at ScienceDirect

Applied Geochemistry

journal homepage: www.elsevier.com/locate/apgeochem

Behaviour of Mo(VI), Eu(III) and U(VI) in calcium-silicate-hydrate phases: Immobilisation and dynamic remobilisation under repository-relevant conditions

Aaron Haben *, Nico Bachmann, Jan Jakob Langer, Ralf Kautenburger

WASTe - Elemental Analysis Group, Inorganic Solid State Chemistry, Saarland University, Saarbrücken, Germany

ARTICLE INFO

Editorial handling by: Elisa Sacchi

Keywords:
C–S–H
High-level nuclear waste
Molybdenum
Europium
Uranium
Mini-column experiments
Remobilisation dynamics
ICP-QQQ

ABSTRACT

Calcium-silicate-hydrate (C–S–H) phases play an essential role as a geotechnical barrier in high-level nuclear waste (HLW) repositories. To guarantee the long-term safety of a HLW disposal site, it is important to know how and to which degree radionuclides are retained by C–S–H phases. To this date, only little to no data on the remobilisation dynamics of the repository-relevant elements Mo(VI), Eu(III) and U(VI) under realistic conditions are available. In this study, C–S–H phases incorporating these elements were synthesised, the element immobilisation was quantified via ICP-QQQ and their structure was investigated via X-ray diffractometry. All C–S–H phases had a calcium-silicon ratio (C/S) of 1.066 ± 0.003 and no relevant structural influences of the studied elements could be observed. In all cases, quantitative immobilisation was observed for Eu(III) and U(VI), whereas Mo(VI) was retained/incorporated to only about 50 %. Afterwards, their leaching behaviour with ultrapure water was studied in batch and mini-column experiments (MCE). Mo(VI) was remobilised quickly, while Eu(III) and U(VI) were retained nearly quantitatively. Due to the more realistic and therefore more representative conditions, further experiments to investigate the effects of three repository-relevant parameters were conducted only using MCE. A higher ionic strength significantly enhanced U(VI) remobilisation, while Eu(III) and Mo(VI) remained nearly unaffected. The displacement agents Fe(III) and Tb(III) only affected Mo(VI)'s remobilisation by retarding it. The addition of a complexing agent (2-phosphonobutane-1,2,4-tricarboxylic acid; PBTC) led to a delayed remobilisation of Mo(VI), while Eu(III) and U(VI) were remobilised to some degree after sufficient PBTC eluation. Overall, this work delivers important information on key processes relevant to nuclear waste disposal.

1. Introduction

With the discovery of radioactivity, numerous new technologies emerged to harness radioactive processes but also brought the challenge of disposing the resulting high-level nuclear waste (HLW). This mainly involves spent fuel elements from nuclear power plants, waste from the reprocessing of these and material from decommissioned nuclear weapons (Oelkers and Montel, 2008). To effectively protect future generations from the harmful effects of radionuclides and their fission products, the final storage of HLW in deep geological formations is envisaged (Kautenburger and Beck, 2008; Freiesleben, 2013; Jobmann et al., 2017; Lommerzheim et al., 2019). Cement-based materials are a crucial component in such future HLW, but also in intermediate (ILW) and low-level waste (LLW) repositories. Due to their physical and chemical stability and their ability to immobilise hazardous substances, they are used as construction or sealing materials (Atkins et al., 1992; Evans, 2008; Ochs et al., 2016; Luhar et al., 2023). Therefore, understanding the retention behaviour of repository-relevant elements under geochemical conditions on cement phases is of great interest.

In contact with penetrating pore water hydrated cement is not thermodynamically stable. This results in cement aging phases, which consist essentially of calcium silicate hydrate (C–S–H) phases. Since the majority of both freshly hydrated and aged cement consists of C–S–H phases and they are considered to be responsible for the heavy metal binding ability of cementitious materials, they are crucial for the safety assessment in repository research (Spence, 1993; Gaona et al., 2011; Ochs et al., 2016; Baur et al., 2022). In contact with aqueous media C–S–H Phases degrade, whereby the molar calcium to silicon (C/S) ratio decreases within approx. 36,000 years from 1.5 to 0.8 due to the leaching of Ca(II) (Jacques et al., 2009; Baston et al., 2012). The

* Corresponding author. at: Inorganic Solid State Chemistry – WASTe - Elemental analysis group, Campus C4.1, 66123, Saarbrücken, Germany.
E-mail address: aaron.haben@uni-saarland.de (A. Haben).

https://doi.org/10.1016/j.apgeochem.2026.106684
Received 29 August 2025; Received in revised form 22 December 2025; Accepted 5 January 2026
Available online 5 January 2026

resulting pore water has an alkaline pH of about 12.5, which decreases with decreasing C/S ratio to approximately 10. The alteration of the C–S–H phases is very complex, particularly due to their semi-crystalline structural characteristics and the involved dissolution and precipitation reactions (Baston et al., 2012; Lothenbach and Nonat, 2015; Papatzani et al., 2015; Ochs et al., 2016). C–S–H phases synthesised by co-precipitation are predominantly described as a semi-crystalline cement gel with either a 11 Å or 14 Å tobermorite structure (Richardson, 2008; Baston et al., 2012; Papatzani et al., 2015; Kee et al., 2021). Thereby structural models by Grangeon et al. (2016) suggest that an increasing Ca(II) content leads to enhanced Ca^{2+} intercalation within the tobermorite interlayers and, at even higher C/S ratios, to the formation of $Ca(OH)_2$ both and outside the C–S–H structure. Despite these complexities, C–S–H phases remain the principal sorbing component of cementitious barriers throughout repository evolution.

Radionuclides originating from the near field of the disposal site can be adsorbed or even incorporated into the C–S–H structure of the surrounding geotechnical barriers (Ochs et al., 2016). Among these, uranium, as one of the main components of spent nuclear fuel, is of particular interest (Motta et al., 2015; Brix et al., 2023). In C–S–H phases it is primarily present in the oxidation state + VI (Harfouche et al., 2006; Macé et al., 2013; Wolter et al., 2019). Many studies have observed high U(VI) retention via surface complexation, incorporation into the C–S–H structure, precipitation, or the formation of ternary Ca(II)–U(VI) surface species/phases (Evans, 2008; Tits et al., 2008, 2011, 2015; Baqer et al., 2023; Macé et al., 2023). Androniuk et al., for example, identified mono- and bidentate outer-sphere complexes of UO_2^{2+} with the deprodtonated oxygen atoms of the bridging Si(IV)-tetrahedra. Thereby, due to the sorption of Ca^{2+} ions on the same sorption sites, a competition between UO_2^{2+} and Ca^{2+} has been suggested (Androniuk et al., 2017; Androniuk and Kalinichev, 2020). Despite the formation of negatively charged aqueous U(VI) species at pH > 10, the U(VI) retention by C–S–H gel increases with increasing C/S ratio, suggesting a U(VI) uptake mechanism involving Ca^{2+} from the C–S–H interlayers (Pointeau et al., 2004; Wolter et al., 2019; Macé et al., 2023).

Europium is an important radionuclide in the context of nuclear decommissioning (Efremenkov and Drace, 2007) and is often used as a less toxic and non-radioactive homologue for the trivalent actinides Cm(III) and Am(III) (Eisenbud et al., 1984; Krauskopf, 1986; Tits et al., 2003). Pointeau et al. (2001) have shown that Eu(III) is nearly quantitatively immobilised by C–S–H, mainly by substitution of Ca^{2+} in the C–S–H structure, and by near-surface complexation or precipitation. In this context, it was shown that no precipitation of Eu(III) hydroxide was observed and thus sorption to C–S–H dominated the retention mechanism, while a higher C/S leads to a stronger binding of Eu(III). These results thus reflect the rest of the literature; with one important exception: in other publications, in a pH range >10, precipitation is indeed reported as part of the retention (Tits et al., 2003; Mandaliev et al., 2011; Kee et al., 2021; Baur et al., 2022; Burešová et al., 2023; Dettmann et al., 2023). Furthermore, Kee et al. (2021) have shown that the incorporation of Eu(III) during C–S–H synthesis significantly inhibits crystal growth and reduces particle size.

For molybdenum, only limited retention on C–S–H phases is reported. Ochs et al. (2016) (and sources within) and Lange et al. (2020) reported a measurable contribution of C–S–H phases to the total retention of Mo(VI) in Portland cement, with increased retention at higher C/S ratios. This is attributed to electrostatic adsorption on a positively charged C–S–H surface (C/S ≥ 1.2) and is therefore associated with a strong pH influence: OH^- and MoO_4^{2-} can compete for those sorption sites. In structural studies, Caselles et al. (2021) were unable to detect any changes in the C–S–H structure due to incorporated Mo(VI). However, they identified the precipitation of powellite ($CaMoO_4$) as the main retention mechanism. It can therefore be assumed that the increasing Mo (VI) retention with a higher C/S is due to a larger number of electrostatic sorption sites as well as a higher Ca(II) concentration and thus a favoured powellite precipitation. Notably, Grambow et al. (2020) negatively highlighted substantial inter-laboratory variability in Mo(VI) retention data, underlining the need for further studies.

Despite the extensive body of literature on retention mechanisms (mainly for Eu(III) and U(VI)), data on the remobilisation or leaching of radionuclides from C–S–H phases remain scarce. For Mo(VI) and Eu(III) remobilisation or leaching, no valid literature data is available, while the existing data for U(VI) are limited and insufficiently representative regarding the conditions for potential repositories. The influence of repository-relevant factors (e.g. ionic strength, competition-/displacement ions or cement additives) has not been sufficiently investigated. Moreover, previous investigations exclusively relied on static batch experiments, which can only approximate conditions expected in a repository environment. Dynamic column experiments provide a more realistic representation of radionuclide transport and leaching behaviour but are often resource-intensive and therefore rarely applied. Haben et al. (2024) have recently presented a remedy in the form of mini-column experiments (MCE). This approach enables systematic investigation of remobilisation processes under controlled flow conditions while minimising experimental effort.

The present work is intended to address all the described gaps in knowledge by investigating the retention, structural effects, and dynamic remobilisation of radionuclides from C–S–H phases under repository relevant conditions. Therefore, C–S–H phases with incorporated Mo(VI), Eu(III) and U(VI) were synthesised, both as single elements and as a mixture, in two different concentrations. After quantifying the retention and analysing the structural effects, the radionuclide remobilisation was investigated. Therefore, standardised batch and dynamic MCE were conducted in ultrapure water. Subsequently, the influence of the ionic strength of the electrolyte (up to 2 M NaCl; depending on disposal side up to 5 M are conceivable; Brix et al. (2021) and sources within), the influence of the cement additive PBTC (2-phosphonobutane-1,2,4-tricarboxylic acid) as potential complexing agent (Rickert and Thielen, 2004; Kretzschmar et al., 2022) and the potential displacement by Fe(III) and Tb(III) were investigated. In many countries (including Germany), the HLW container is to be made of a steel alloy, what inevitably leads to corrosion of the alloy and thus to large amounts of Fe(III) ions in the vicinity of the repository (Féron et al., 2008; Burger et al., 2013; Dörr et al., 2013; Shrestha et al., 2021; Feng et al., 2024). Regarding Tb(III): Due to the chemically similar behaviour of the trivalent lanthanides (*Ln*) and actinides (*An*), it is common practice in nuclear science to investigate the behaviour of *Ln* as a stable substitute for *An* (Cross et al., 2016; Ochs et al., 2016; Welch et al., 2017). Because of the high similarities the Ln group (Cotton, 2006; Hege et al., 2024) Tb(III) is therefore particularly interesting as a displacement ion for Eu(III).

Based on the dynamic experimental approaches, this study provides new mechanistic insights into radionuclide remobilisation from C–S–H phases and demonstrates the practicality of MCE as an efficient tool for repository research.

2. Materials and methods

2.1. Chemicals

Ultrapure water (0.055 μS cm^{-1}) (PURELAB® Chorus 1 ultrapure water filtration unit, Elga LabWater, High Wycombe, UK) was used to prepare all solutions. NaCl with premium-grade quality (EMSURE®) from Merck (Darmstadt, Germany) was used to prepare the eluents for MCEs and the electrolytes for the batch experiments. HNO_3 (Rotipuran® Supra 69 %, Carl Roth, Karlsruhe, Germany) was used to acidify the measurement solutions, whereas HCl (30 % Suprapur®, Merck Supelco®, Darmstadt, Germany) and NaOH (Suprapur® 30 %, Merck, Darmstadt, Germany) were used to adjust the pH in the experiments. For the displacement and leaching experiments Fe(III) (1 g L^{-1} in 2–3 % HNO_3, Merck Certipur®, Darmstadt, Germany) and Tb(III) (10 g L^{-1} in 2 % HNO_3, AccuStandard, New Haven, USA) inductively coupled

plasma mass spectrometry (ICP-MS) standard solutions and a 50 wt% PBTC solution (2-Phosphonobutane-1,2,4-tricarboxylic Acid, TCI, Tokyo, Japan) were used. A solution with 10 mg L^{-1} of Sc(III) (1 g L^{-1} in 5 % HNO_3, Alfa®, Karlsruhe, Germany), Y(III) (1 g L^{-1} in 2–3 % HNO_3, Merck Certipur®, Darmstadt, Germany) and Ho(III) (1 g L^{-1} in 2–3 % HNO_3, Merck Certipur®, Darmstadt, Germany) in 5 % HNO_3 was prepared as the internal standard stock solution for all inductively coupled plasma triple quadrupole mass spectrometry (ICP-QQQ) measurements. Argon 5.0 (Ar ≥ 99.999 mol%, ALPHAGAZ™ 1 Argon, Air Liquide, Düsseldorf, Germany) was used as plasma gas for ICP-QQQ measurements. For the experiments and ICP-QQQ calibration, Mo(VI) (1 g L^{-1} in 1 mol L^{-1} with traces HF, Bernd Kraft, Duisburg, Germany), Eu(III) (10 g L^{-1} in diluted HNO_3, Agilent, Kingstown, USA) and U(VI) (1 g L^{-1} in 2–5 % HNO_3, AccuStandard, New Haven, USA) ICP-MS standard solutions were used. Furthermore, Ca(II) (1 g L^{-1} in 0.5 mol L^{-1} HNO_3, Merck Certipur®, Darmstadt, Germany) and Si(IV) (10 g L^{-1} in water. Tr. HF, AccuStandard, New Haven, USA) standards were used for ICP-QQQ calibration of the leaching experiments.

2.2. Synthesis of the C–S–H phases

The most common synthesis route for C–S–H phases is the co-precipitation from an aqueous solution/suspension with CaO and SiO_2 as precursors (Atkins et al., 1992; Tits et al., 2006; Gaona et al., 2011; Wolter et al., 2019; Kee et al., 2021). According to Grangeon et al. (2016), it can be assumed that, starting from a pure tobermorite structure (at C/S = 0.67), an increase of the C/S ratio leads to increased Ca^{2+} intercalation into the tobermorite interlayer and ultimately to the precipitation of $Ca(OH)_2$. At a C/S < 1.5, $Ca(OH)_2$ still forms within the tobermorite structure, while at C/S > 1.5 it also forms outside the crystal structure. Since the focus of this work is on the different of "external" conditions relevant to a repository and not on the effects of varying C/S ratios, a decision had to be made on one C/S ratio. Taking the above into account, a C/S between 0.67 and 1.5 is advisable. Therefore, a C/S of 1.07 was chosen here (CaO to SiO_2 mass ratio of 1).

For the synthesis of the C–S–H phases, CaO (≥99.95 %, metals basis, Thermo Scientific, Darmstadt, Germany) and SiO_2 (Aerosil® 300, SiO_2≥99.8 %, BET 270–330 m^2 g^{-1}, Evonik Operations, Essen, Germany) were mixed with ultra-pure water in 50 mL centrifuge tubes (Ultra-High Performance Centrifuge Tubes, PP, 20000g, VWR, Randor, USA) with a solid to liquid ratio (S/L) of 50 g L^{-1} and a C/S of 1.07. The reaction mixture was shaken in a rotary shaker (Stuart®, Rotator SB3, Cole-Parmer®, Vernon Hills, USA) at 40 rounds per minute for 4 weeks under Ar atmosphere (Ar ≥ 99.999 mol%, ALPHAGAZ™ 1 Argon, Air Liquide, Düsseldorf, Germany). They were then centrifuged for 30 min at 16990g (centrifuge 3-18 KS, Sigma, Osterode am Harz, Germany), the supernatant was decanted under Ar atmosphere and stored for further investigation. The solid phases were then dried under vacuum in a desiccator over silica gel until the weight remained constant.

For the incorporated C–S–H phases, Mo(VI), Eu(III) or U(VI) were added solo ("Mo-y", "Eu-y", "U-y") or as a mixture (Waste Cocktail; "WC-y") to the reaction mixture. The analyte solutions were pH-neutralised in advance. In all cases, two different concentrations for each analyte in the reaction mixture was chosen: $5•10^{-5}$ mol L^{-1} ("x-L") and $5•10^{-4}$ mol L^{-1} ("x-H"). An additional batch was subsequently prepared for the WC sample in the lower concentration ("WC-L_2"), as the initial quantity was not sufficient. The concentrations of the analytes in the "WC-L_2" reaction solution deviate slightly: for Mo(VI) the concentration was $4.64•10^{-5}$ mol L^{-1}, for Eu(III) $5.49•10^{-5}$ mol L^{-1} and for U(VI) it was $5.13•10^{-5}$ mol L^{-1}. Based on a quantitative retention, the added analyte contents result in a maximal possible analyte concentration of $1•10^{-6}$ mol g^{-1} in the in the "x-L" C–S–H phases (slightly different for "WC-L_2") or $1•10^{-5}$ mol g^{-1} in the "x-H" ones.

To determine the exact analyte contents in the respective C–S–H phases, an indirect quantification during and after the synthesis was performed. All used and accumulated supernatant solutions and reaction tubes were analysed towards the corresponding analytes. ICP-QQQ quantification was performed as described in Chapter 2.6.

2.3. XRD measurement

Powder X-ray diffraction (PXRD) patterns of the different samples were recorded at room temperature on a D8-A25-Advance diffractometer (Bruker, Karlsruhe, Germany) in case of air-stable samples, while air-sensitive samples were measured on a X'Pert MPD diffractometer (PANalytical, Almelo, Netherlands) using dome sample holders. In both cases, measurements were performed in Bragg-Brentano θ-θ-geometry (goniometer radius D8 280 mm; MPD 240 mm) with Cu K_α-radiation (λ_1 = 154.0596, λ_2 = 154.4426 p.m.), as well as a 12 μm Ni foil working as K_β filter and a variable divergence slit at the primary beam side. A LYNXEYE detector with 192 channels was used at the secondary beam side on the D8-A25-Advance and a PIXcel^{1D} detector on the X'Pert MPD diffractometer. Experiments were carried out in a 2θ range of 7–120° with a step size of 0.013° and a total scan time of 2 h.

2.4. Mini column experiments (MCE)

The column experiments carried out are based on the recently published MCE method by Haben et al. (2024). This method allows the execution of extremely resource- and time efficient leaching experiments. The mini columns used are HPLC guard columns (UPC–130B, UPCHURCH SCIENTIFIC™, Oak Habor, USA), drilled out to 3.5 mm inner diameter, with a 500 nm pore size filter disc (A-103X, UPCHURCH SCIENTIFIC™, Oak Habor, USA). The dry C–S–H phases were filled into the column with a suitable funnel and thereby gradually compacted. The HPLC components used are Agilent 1100, 1200 and 1260 Infinity II HPLC systems (Waldbronn, Germany) and are listed in Table 1.

The MCE were performed with ultrapure water, 0.1 M, 1 M and 2 M NaCl as eluent with a column temperature of 25 °C. The columns were packed with approx. 147 mg of C–S–H (exact weight was considered in the respective experiments) and then preconditioned in the HPLC for 150 min using a flow gradient from 10 to 40 μL min^{-1}. The eluate of the preconditioning step was also collected. After preconditioning, the flowrate of the eluent was set to 40 μL min^{-1}. In total, an MCE experiment lasts 65 h (including preconditioning) with a total pore volume of 154 mL, and for MCE in presence of PBTC, a total of 127.5 h with a total pore volume of 304 mL. Depending on the experiment, 10 μL of either a $1.7•10^{-4}$ mol L^{-1} Fe(III), $1.4•10^{-4}$ mol L^{-1} Tb(III) or $63.6•10^{-3}$ mol L^{-1} PBTC solution were injected multiple times into ultrapure water (eluent) via the autosampler. For Fe(III)-displacement a 100-fold equivalent (over 100 injections), for Tb(III)-displacement also a 100-fold equivalent (over 100 injections) and for the PBTC-leaching a total of 1000-fold equivalent (over 200 injections) were injected; all equivalences are in relation to the amount of Eu(III) on the column. After the column, the entire eluate was collected by means of a fraction collector. Samples were taken from the individual fractions for an ICP-QQQ measurement,

Table 1
Components and software of used HPLC system for MCE.

Hardware:	
1100 Series G1379A Degasser	
1100 Series G1312A Binary Pump	1260 Infinity II G7111B Quaternary Pump
1100 Series G1313A Autosampler	1260 Infinity II G7129A Vialsampler
1100 Series G1316A Column oven	1260 Infinity II G7116A Multicolumn Thermostat
1100 Series G1315B Diode Array Detector	1260 Infinity II G7117C Diode Array Detector
1200 Series G1364C Fraction collector	1200 Series G1364C Fraction collector
Software:	
ChemStation for LC 3D Systems Rev. B.02.01-SR2 [260]	OpenLab CDS ChemStation Edition Rev. C.01.10 [322]

and the pH values were determined (pH-meter SevenMulti, pH-electrode InLab®, Mettler Toledo, Columbus, USA). ICP-QQQ quantification was performed as described in Chapter 2.6.

2.5. Batch experiments

The batch experiments were conducted for additional validation of the still new dynamic MCE method. All leaching experiments in ultrapure water were therefore performed as batch and MCE.

All the batch experiments were prepared in triplicates, where 10 mL of ultrapure water was added to 40.0 ± 0.2 mg of the respective C–S–H phase (S/L = 4 g L^{-1}) in a 15 mL polypropylene (PP) centrifuge tube (Ultra-High Performance Centrifuge Tube, VWR® International, Darmstadt, Germany), followed by equilibration in a horizontal shaker (Promax 1020 platform shaker, Heidolph Instruments, Schwabach, Germany) at room temperature. Every 24 h the pH was measured, 5 mL of sample was taken and subsequently refilled with 5 mL fresh ultrapure water. This was repeated until a total pore water (exchange-) volume of 75 mL was reached. On weekends, the 24-h rhythm could not be maintained, so that the batch experiments extended over a total period of 21 days. ICP-QQQ quantification was performed as described in Chapter 2.6.

2.6. ICP-QQQ measurements

For the ICP-QQQ measurement, an Agilent 8900 ICP-QQQ (Santa Clara, USA) with an Agilent SPS 4 autosampler (Santa Clara, USA) was used. The measurements were performed with the parameters given in Table 2 and with different cell gas modes: ^{28}Si and ^{40}Ca were measured in H_2-reaction gas mode via mass pair (Q_1, Q_2) = (28, 28) and (Q_1, Q_2) = (40, 40). ^{95}Mo, ^{153}Eu, ^{157}Tb and ^{238}U were measured in "NoGas"-mode and ^{56}Fe in He collision gas mode. For quantification, an external calibration was performed.

3. Results and discussion

3.1. Amounts of analytes bound/immobilised to C–S–H

The respective analyte contents of the solid phases can be derived from analysing the elemental contents of the reaction tube walls and the supernatant solutions after C–S–H phase synthesis. These are shown in Table 3. If the resulting C/S is calculated from the values listed there, the average value is 1.066 ± 0.003. Based on the synthesis route described in Chapter 2.2, a C/S of 1.07 would have been expected. Thus, the reproducibility of the C–S–H phase synthesis is excellent.

Based on the absolute amounts added during synthesis and the quantities found in the supernatant and on the tube walls, the proportion bound to/in the C–S–H phases can be calculated for each analyte. The absolute quantities in the fractions "bound," "supernatant," and "tube walls" are listed in the supplementary information in Table S1, and the relative proportions are shown in Fig. S1. For a better overview, only the actual bound/incorporated amounts of substance (R [%]) are shown in Fig. 1. It shows that retention/incorporation values of ≥99.94 % were determined for Si(IV), >98.7 % for Ca(II), between 46.9 % and 59.3 % for Mo(VI), >97.8 % for Eu(III), and >98.9 % for U(VI). Table S1 and Fig. S1 also show where the missing, unbound fractions of the respective analytes are located. In the case of Mo(VI), this was found almost exclusively in the supernatant solution, so that non-incorporation can be assumed; the same applies to Ca(II). In the case of Eu(III) and U(VI), however, a large part of the non-incorporated amount was measured on the tube walls, and in the case of Si(IV), the unbound fraction is divided almost equally between the supernatant and the tube walls. Overall, however, an almost quantitative retention (incorporation) can be assumed for the elements Si(IV), Ca(II), Eu(III), and U(VI). It is also worth mentioning that almost identical R [%] were determined for "WC-L_1" and "WC-L_2", once again underlining the excellent reproducibility of the C–S–H synthesis.

Table 2
Parameters of all ICP-QQQ measurements.

RF Power	1550 W
Plasma gas flow rate	15.0 L min^{-1}
Nebuliser gas flow rate	1.03 L min^{-1}
Integration time	300 ms
Sweeps per replicate	20
Dwell time	15 ms
Replicates	3
H_2/He gas flow	$4.8•10^{-3}$/$4.1•10^{-3}$ L min^{-1}

Table 3
Si(IV), Ca(II), Mo(VI), Eu(III) and U(VI) concentrations (c) in all synthesised C–S–H phases, derived from analyte content in supernatant solution and on reaction tube walls after the C–S–H phase synthesis; Single element phases: "Mo-y", "Eu-y" and "U-y"; Multi element phases: "WC-y"; in low ("x-L") and high ("x-H") concentration; initial concentrations see Chapter 2.2.

C–S–H Phase	c(Si) [mmol g^{-1}]	c(Ca) [mmol g^{-1}]	c(Mo) [μmol g^{-1}]	c(Eu) [μmol g^{-1}]	c(U) [μmol g^{-1}]
U-L	7.566	8.067	–	–	0.905
U–H	7.459	7.934	–	–	8.867
Mo-L	7.582	8.098	0.538	–	–
Mo–H	7.439	7.929	4.829	–	–
Eu-L	7.556	8.073	–	0.888	–
Eu–H	7.582	8.091	–	9.057	–
WC-L_1	7.652	8.164	0.515	0.918	0.919
WC-L_2	7.500	8.002	0.478	0.986	0.921
WC-H	7.652	8.101	4.289	9.187	9.158

As mentioned in the introduction, the retention and incorporation of Eu(III) and U(VI) on/in C–S–H phases is well described in literature, whereas the one for Mo(VI) is only insufficiently described. The literature reports almost quantitative retention for U(VI), caused by precipitation, intercalation into the interlayers, direct surface complexation and the formation of ternary Ca(II)-uranate-like surface precipitates (see Introduction). Similarly, quantitative retention on C–S–H phases is reported for Eu(III), which is mainly immobilised by incorporation into the C–S–H structure (Ca^{2+} substitution) and surface complexation/precipitation. At pH values < 10, sorption dominates, with a higher C/S increasing the binding, whereas at pH values > 10, precipitation is also observed as a retention mechanism (see Introduction). For example, Brix et al. (2023) reported for a distribution ratio (R_d) of approx. 10,000 L kg^{-1} for Eu(III) and approx. 20,000 L kg^{-1} for U(VI) (at S/L = 4 g L^{-1} and C/S = 0.83). To give a better comparison, these literature R_d values must be converted into R [%]. Equation (1) shows how R_d [L kg^{-1}] values are calculated, where V [L] is the volume of the electrolyte, m [kg] the mass of the adsorbent, n_{eq} [mol] the analyte amount in solution and n_{sorb} [mol] the amount of analyte adsorbed/retained. Based on equation (2), the corresponding retention values R [%] can be calculated from the R_d values listed in the literature. In the case of Brix et al. (2023) this results in a quantitative retention for Eu(III) and U(VI), of 98 % and 99 %. When putting the data listed in Table S1 and Fig. 1 (Fig. S1) in context to the literature, there is very good agreement.

$$R_d = \frac{n_{sorb}}{n_{eq}} \cdot \frac{V}{m} \quad (1)$$

$$R = \frac{R_d}{\frac{V}{m} + R_d} \cdot 100\% \quad (2)$$

The assessment of Mo(VI) is somewhat more difficult. There is not only few, but also widely differing retention and incorporation data available. In general, Mo(VI) shows only limited and low retention on C–S–H phases, where a higher C/S leads to an increasing retention. The

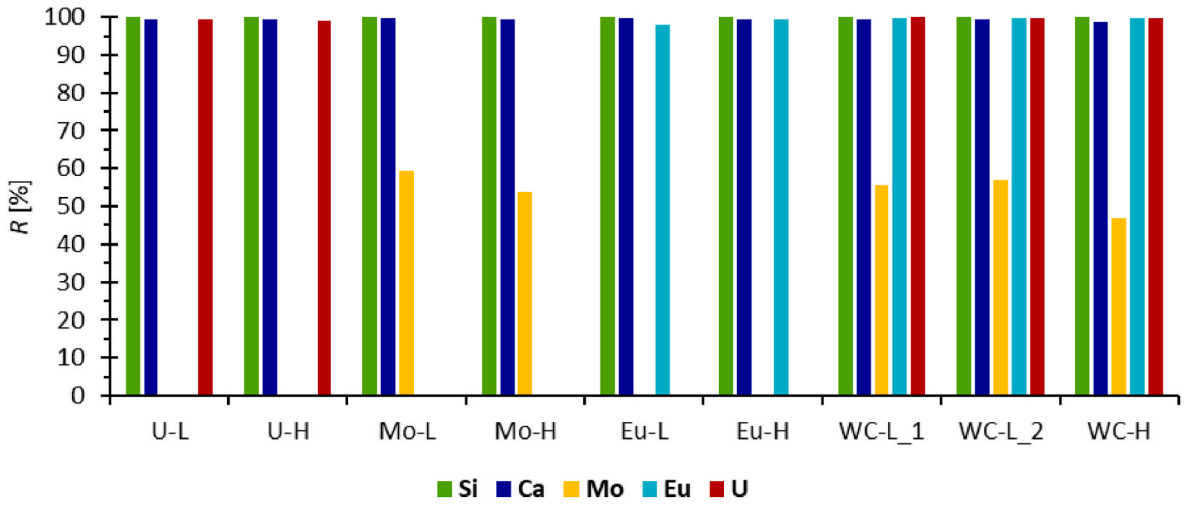

Fig. 1. Percentage retention values (R [%]; relative amounts incorporated and/or bound) of Si(IV), Ca(II), Mo(VI), Eu(III) and U(VI) in/on the synthesised C–S–H phases (values from Fig. S1); nomenclature see Table 3.

increased retention at higher C/S ratios (C/S $\geq$ 1.2) is probably due to the higher number of electrostatic sorption sites and the higher Ca^{2+} concentration, which favours powellite precipitation ($CaMoO_4$) (see Introduction). For example, Lange et al. (2020) report R_d values of approx. 430 L kg^{-1} with an S/L of 40 g L^{-1} and a C/S of 0.9. However, the retention mechanism is not clearly explained, although adsorption is suspected. Grambow et al. (2020) refer, in part, to the data described by Lange et al. (2020) and define an R_d range of 4–430 L kg^{-1} (C/S = 0.8–0.9). Caselles et al. (2021) can be used as a further reference, with reservations. Here, an R_d of approx. 1000 L kg^{-1} was determined at a C/S of 1.6, but this time the precipitation of $CaMoO_4$ is considered the main retention mechanism. In view of the significantly higher C/S, this result also fits very well into the picture. Converting those data using equation (2), this results in a Mo(VI) retention on C–S–H of approx. 6 %–95 % at a S/L of 5 g L^{-1} to 40 g L^{-1} and a C/S of 0.8–1.6. Thus, it can be stated that the retention mechanism of Mo(VI) on C–S–H phases as well as its quantification is only insufficiently described. Literature therefore does not provide an adequate comparison, and the values determined here must be considered in isolation for the time being. The underlying mechanisms are explained in more detail in Chapter 3.3.

3.2. Structural analysis

If the structure of C–S–H phases needs to be assigned, this is not always easy due to the semi-crystalline properties. Fig. 2 shows the diffractograms of a C–S–H phase without ("C–S–H") and a one with the incorporated elements ("WC-H″). Even without a detailed data analysis/refinement, a classification of the solid phases is possible. The structure of C–S–H phases and thus corresponding XRD data are reported in several publications. Both solid phases show the typical, literature-known reflexes (*) (Caselles et al., 2021; Kee et al., 2021; Baur et al., 2022). Furthermore, no differences were observable between the solid phases investigated. Based on the work of Grangeon et al. (2013), the reflexes at 2θ ≈ 17°, 29°, 32° and 50° can be considered as an evidence for a 11 Å tobermorite structure; more specifically a disordered 11 Å tobermorite structure. According to Kee et al. (2021), it is the reflex at 2θ ≈ 7°, that allows the clear identification as 11 Å tobermorite. However, it should also be mentioned that the tobermorite structure can only be expected in the C–S–H synthesis route chosen here (co-precipitation). In a hydrothermal process, for example, a xonotlite structure is reported (Kee et al., 2021).

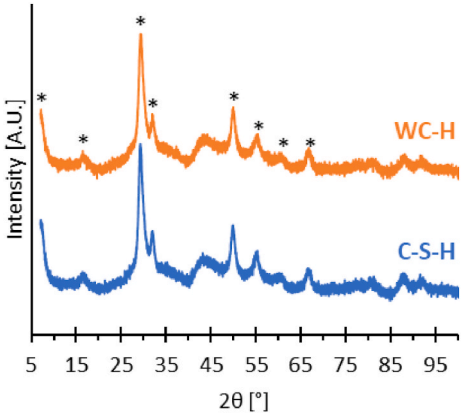

Fig. 2. X-ray diffractograms of the C–S–H phases without ("C–S–H") and with incorporated analytes ("WC-H″ sample; see Table 3).

3.3. Remobilisation in ultrapure water

The remobilisation of the analytes from the synthesised C–S–H phases in ultrapure water will now be discussed. For this purpose, the remaining amounts in [%] of Mo(VI), Eu(III) and U(VI) in the "WC-H″ solid phase (relative to the initial values listed in Table 3) derived from batch and MCE experiments are shown in Fig. 3. The presentation of Si(IV) and Ca(II) is deliberately omitted in Fig. 3, as it would be detract

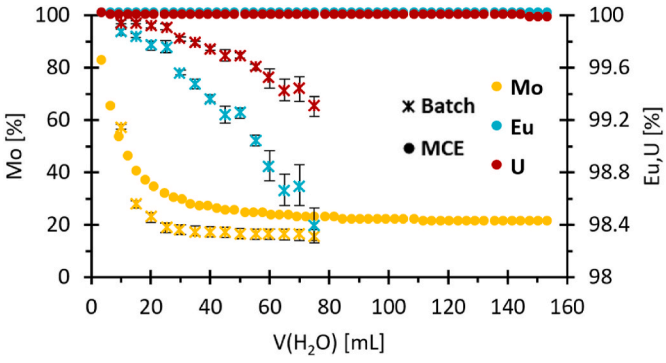

Fig. 3. Remaining Mo(VI), Eu(III) and U(VI) [%] in "WC-H″ sample (see Table 3) plotted against pore water volume during batch- and MCE-leaching experiments.

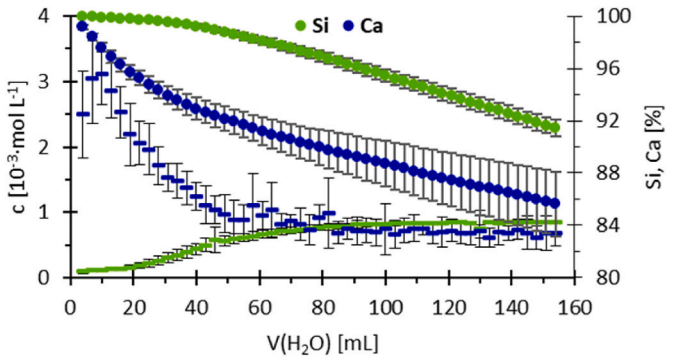

Fig. 4. Leached Si(IV) and Ca(II) concentrations (bars) as well as remaining Si(IV) and Ca (II) ammounts in [%] (dots) averaged over all MCE experiments plotted against the eluent volume (H_2O).

from clarity and will be discussed in more detail in Fig. 4. Additionally, the leached amounts [%] of all analytes in all experiments with ultrapure water are listed in Table 4.

Looking at Fig. 3, it is immediately apparent that all analytes in the "WC-H″ sample leach significantly more in the batch experiments compared to the MCE setup. The same is true for all the other leaching experiments in ultrapure water (see Table 4). This fact becomes more striking in view of the used pore water/elution volume; less was used in the batch experiments (75 mL) compared to MCE (154 mL). Two reasons can be assumed for this: Firstly, depending on the experimental set-up, different "chemical equilibria" can be assumed. While the batch experiments are static systems, where each leaching step equilibrates for at least one day (in total 21 d), the MCE setup can be considered as dynamic; the eluent flows through the column continuously (in total 65 h). Therefore, the longer equilibration time in the batch, could be considered as one reason for the differences in the leaching behaviour. Another possible reason could be the different S/L of the two experimental conditions. While the pore water in the MCE can only occupy the space/pores in the solid phase and can therefore be regarded as natural or realistic, the S/L in batch experiments can only be regarded as an approximation. In the batch setup, there is way more electrolyte available for equilibrium than in the MCE setup. The consideration of equation (1) can mathematically substantiate this hypothesis: If a reasonably constant R_d value for the retention on C–S–H phases is assumed in both experimental setups, a higher electrolyte volume (V) results in a lower value for n_{sorb} (and vice versa results in a higher value for n_{eq}). To further substantiate the influence of the S/L, the work of Wang et al. (2009) can be used. By investigating sorption behaviour of caesium on granite (in batch experiments) and by comparing their results with those from Li et al. (2009) (using columns), they reported that the S/L ratio was probably the decisive factor in the different results obtained from batch and column experiments. Thus, the combination of longer equilibration times and lower S/L leads to a stronger pronounced remobilisation in the batch setup.

Regarding U(VI), in all experiments extremely low remobilisation was observed (both batch and MCE) (see Table 4). Thus, in connection with H_2O, one can speak of a nearly quantitative retention. Although no literature data on dynamic remobilisation studies could be found, the results are in excellent agreement with those of retention/adsorption studies. Quantitative retention of U(VI) on C–S–H phases is generally reported, with remobilisation only increasing due the formation of soluble carbonate species (Wolter et al., 2019; Maragkou and Pashalidis, 2022; Schmeide et al., 2025). However, as already mentioned, there is a difference in the leaching behaviour when comparing batch experiments and MCE, especially in the "x-H" samples. For example, in the "WC-H″ sample (see Fig. 3 and Table 4) 0.7 % of the original U(VI) amount was leached in the batch, whereas only 0.02 % was leached in the MCE. The reason that this difference in U(VI) leaching is more pronounced in the "x-H" samples can be explained by the involvement of different retention mechanisms. Those with significantly higher R_d values could dominate in the "x-L" samples, so that a change in the S/L has a less significant effect.

In the MCE setup, a marginally lower remobilisation can be determined for Eu(III) compared to U(VI) (see Fig. 3 and Table 4). Conversely, Eu(III) leaching is significantly increased in the batch experiments. The same assumption can be made here as above for U(VI), with the difference, that in the case of Eu(III) the effect of a higher electrolyte volume is clearly noticeable in both, the "x-L" and "x-H" samples. No literature data on leaching from C–S–H phases are available for Eu(III), Am(III) or Cm(III). However, to create a literature comparison, the publication by Goo et al. (2021) can be used. They investigated Eu(III) leaching from Portland cement and reported very little to almost no Eu(III) remobilisation.

As already mentioned, significantly stronger pronounced leaching of Mo(VI) can be observed in the batch experiments compared to the MCE. The reasons are analogous to the other analytes. Much more interesting at this point is the kinetic of the Mo(VI) leaching itself. At the beginning, Mo(VI) is remobilised very quickly and to a large extent, whereas towards the end it is leached very slowly. This observation suggests that at least two different retention/remobilisation mechanisms are involved. Based on the curve shown, a comparatively weak adsorption and either strong incorporation or precipitation is obvious. If the solubility product of powellite ($CaMoO_4$) is considered, precipitation can be assumed as the most likely process. During the synthesis, $4.46 \bullet 10^{-1}$ mol L^{-1} CaO and either 50 or $500 \bullet 10^{-6}$ mol L^{-1} MoO_4^{2-} are used (see Chapter 2.2). Based on the pK_{SP} value of 7.72 ($K_{SP} = 1.91 \bullet 10^{-8}$ mol^2 L^{-2}) reported by Essington (1990), $CaMoO_4$ precipitation can therefore be expected. Even with the Ca(II) and Mo(VI) concentrations in solution at the beginning of the leaching experiments itself, this solubility product is still exceeded. For example, in the MCE experiment described in Fig. 3, $3.99 \bullet 10^{-3}$ mol L^{-1} Ca(II) (see Fig. 4) and $3.07 \bullet 10^{-5}$ mol L^{-1} Mo(VI) (see supplementary data Fig. S2) were measured in the first fraction (product = $1.22 \bullet 10^{-7}$ mol^2 L^{-2}). This observation is also confirmed by Caselles et al. (2021). There, co-precipitation as $CaMoO_4$ is postulated as the main retention mechanism, although the possibility of surface adsorption could not be ruled out. However, no proof was provided. Here, on the other hand, the remobilisation kinetics visible in Fig. 3 can be regarded as strong indication for a combination of weak surface adsorption and the precipitation of $CaMoO_4$.

Apart from the differences between batch and MCE, the leaching behaviour of Si(IV) and Ca(II) agrees with literature data. In summary, it can be said that C–S–H phases with a C/S < 0.83 initially leach more Si(IV), whereas C–S–H phases with a C/S > 0.83 initially leach more Ca(II). If a C/S = 0.83 is reached in both cases, the C–S–H phases dissolve congruently (Si(IV) and Ca(II) leach to the same extent) (Baston et al., 2012; Walker et al., 2016). Based on the C/S of 1.066 ± 0.003 averaged from Table 3, increased Ca(II) leaching would be expected at

Table 4
Amounts of remobilised analytes in [%] (in relation to the values listed in Table 3) at the end of the leaching single element (SE) and multi element (WC) experiments in ultrapure water; C–S–H with low (L) and high (H) analyte concentration; amount of pore water in batch setup = 75 mL and in MCE setup = 154 mL.

			Amounts leached [%]				
			Mo	Eu	U	Si	Ca
Batch	SE	L	75.5	1.34	0.35	11.1	16.8
		H	83.5	1.00	0.60	10.9	17.3
	WC	L	76.1	2.22	0.62	11.4	16.5
		H	84.0	1.61	0.70	9.9	17.8
MCE	SE	L	72.3	0.11	0.42	8.6	13.3
		H	74.6	<0.01	0.02	8.6	14.6
	WC	L	72.9	0.02	0.08	8.5	17.1
		H	79.8	<0.01	0.02	7.1	14.2

the beginning. Fig. 4 shows both, the concentrations and the remaining quantities of Si(IV) and Ca(II) plotted against the elution volume; both averaged over all MCEs with ultrapure water. In fact, a high Ca(II) concentration (over $3\bullet10^{-3}$ mol L^{-1}) was measured in the first fractions, which decreases up to a pore volume of 80 mL (approx. $7\bullet10^{-4}$ mol L^{-1}). The reverse is true for Si(IV). The measured Si(IV) concentration increases up to a pore volume of 80 mL: from initially below $1\bullet10^{-4}$ to approx. $8\bullet10^{-4}$ mol L^{-1}. Since the measured Si(IV) and Ca(II) concentrations can be regarded as constant from an H_2O volume of 80 mL, congruent leaching can also be assumed here. However, it should also be mentioned that the Ca(II) leaching was significantly less reproducible and more error-prone than that for Si(IV) (see Fig. 4). As discussed above, Ca(II) is suspected to be more involved in the retention mechanisms of the other analytes and is therefore also subject to greater fluctuations due to different analyte leaching and possible re-immobilisation (such as co-precipitation after leaching).

There were no significant differences in the measured pH values. In the batch, an average pH of 11.3 ± 0.1 was determined at the beginning of the experiments and a pH of 10.84 ± 0.07 at the end. In the MCE, the average pH was 11.73 ± 0.09 at the beginning and 10.78 ± 0.07 at the end of the experiments (same can be seen for MCEs described below; supplementary Figures S3, S5 and S8). The marginally higher initial pH in the MCE can again be explained by the significantly higher S/L ratio. The reason for the decrease in pH values over the duration of the experiments lies in the Ca(II)-leaching. Since all C–S–H phases leach significantly more Ca(II) (compared to Si(IV)), it can be assumed that the C/S decreases over the course of the experiment and thus the pH of the pore water also decreases (see Introduction).

3.4. Remobilisation in dependence of ionic strength

Based on the results and interpretations from Chapter 3.3, it was concluded that the implementation of MCE leaching experiments reflects natural conditions better than batch experiments. For this reason, no batch experiments were conducted when investigating the effects of different ionic strengths; the same applies for all later sections.

Fig. 5 shows the leaching curves of Mo(VI), Eu(III) and U(VI) from the incorporated "WC-L_1" C–S–H phase for different ionic strengths (0–2 M NaCl). For better comparability, the resulting leached quantities are listed in Table 5.

Neither for Mo(VI) nor for Eu(III) any significant influence of the ionic strength on the leaching behaviour can be observed. A comparison of the values for ultrapure water and those for different ionic strengths shows no differences (within the limits of the fluctuation ranges). From Table 4, an averaged leaching of 75 % ± 3 % can be determined for Mo(VI) over all MCE in ultrapure water; for Eu(III) 0.03 % ± 0.05 %. Compared with the values from Table 5, an averaged value of 75 % ± 3 % results for Mo(VI) and 0.02 % ± 0.00 % for Eu(III) in different ionic

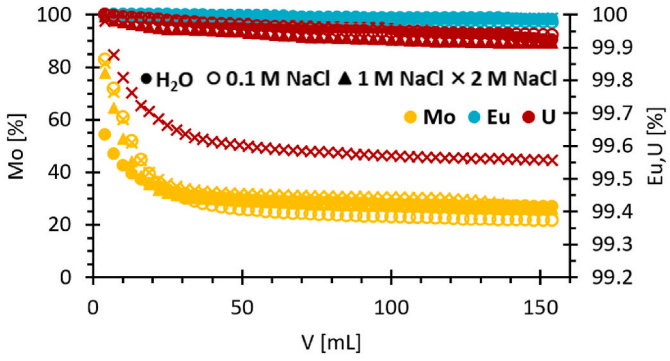

Fig. 5. Remaining Mo(VI), Eu(III) and U(VI) [%] in "WC-L_1" sample (see Table 3) plotted against pore water volume in different ionic strength solutions; all were conducted as MCE-leaching experiments.

Table 5
Amounts of remobilised analytes in [%] from "WC-L_1" (in relation to the values listed in Table 3) at the end of MCE leaching experiments with different ionic strength (data from Fig. 5 and S4); each after 154 mL elution volume.

Eluent	Leached amount [%]				
	Si	Ca	Mo	Eu	U
H_2O	8.5	17.1	72.9	0.02	0.08
0.1 M NaCl	14.9	24.9	78.4	0.02	0.06
1 M NaCl	25.3	33.7	73.7	0.01	0.09
2 M NaCl	12.5	28.9	75.1	0.01	0.44

strengths. In view of the results for Si(IV) and Ca(II) leaching (see next paragraph), a Ca(II)-mediated sorption on or in the C–S–H structure thus seems rather unlikely for Mo(VI) and Eu(III).

The Si(IV) and Ca(II) leaching curves (analogous to Fig. 5), the measured Si(IV) and Ca(II) concentrations and the measured pH are listed in the supplementary data (Fig. S3 and S4). Fig. S3 also shows that the ionic strength does not influence the pH in any way. For Si(IV), the total leached amount increases from 8.5 % in ultrapure water to 25.3 % in 1 M NaCl; in the case of Ca(II) from 17.1 % to 33.7 % (see Table 5 and Fig. S4). Subsequently, in the step from 1 M to 2 M NaCl, the leached amount decreases again: for Si(IV) to 12.5 % and for Ca(II) to 28.9 %. The increased Ca(II) leaching with higher NaCl concentration is in excellent agreement with the literature. Wolter et al. (2019) conducted batch experiments and have measured a similar tendency for Si(IV) and Ca(II) as a function of ionic strength but unfortunately failed to provide any explanation. Glasser et al. (2005) have shown that the Ca(II) solubility increases significantly up to an ionic strength of 1.5 M NaCl. The increase in Ca(II) solubility is mainly attributed to the formation of calcium chlorido complexes. Hill et al. (2006) and Sugiyama (2008) also report an increased Ca(II) release with increased ionic strength. In contrast, they postulated a cation exchange of Ca^{2+} by Na^{+} as the decisive mechanism.

The leaching behaviour of Si(IV) and Ca(II) at ionic strengths above 1.5 M NaCl is barely reported in the literature. In particular, the decrease in leaching behaviour between 1 M and 2 M NaCl observed by us has not been described previously. Our results show a clear decrease in leaching between 1 M and 2 M NaCl, which contradicts the few available literature data on Si(IV) solubility. Glasser et al. (2005) found hardly any influence of increasing NaCl concentrations (up to 1.46 M) on Si(IV) solubility, more so, they report that at low C/S (0.85) the Si(IV) solubility should be slightly reduced by increasing aqueous NaCl concentrations. This observation is in clear contradiction to the values in Fig. S4/Table 5 and Fig. S3. Due to the insufficient data and lack of specific experiments at this ionic strength, there are various potential explanations for this phenomenon. The most plausible would be that Ca^{2+} is not only substituted in the interlayer, but also at SiO_4^{4-} tetrahedron-bridging sites. This would partially break up the C–S–H structure, resulting in increased Si(IV) leaching; in form of silicate mono-, oligo- and polymers. This idea would result in silicate agglomerates forming and precipitating from a certain threshold value of monomers, oligomers or polymers. Accordingly, this threshold value of silicate species in the eluate would be reached between 1 M NaCl and 2 M NaCl. If silicate agglomerates were to form in addition to the C–S–H phases in the saline solution, this would create new sorption sites for cations such as Ca^{2+}. This would also explain the slight decrease in Ca(II) leaching from 1 M to 2 M NaCl.

In the case of U(VI), Table 5 and Fig. 5 show an influence only at an ionic strength of 2 M NaCl. Thus, from 1 M to 2 M NaCl, the amount leached increases in by a factor of 5. With that, a relatively large increase is visible, whereas in absolute terms one can still speak of near quantitative retention. These results contradict the ones of Wolter et al. (2019). They reported that an increased ionic strength leads to increased Ca(II) leaching and with that affects the structural integrity of C–S–H phases but has no to negligible effect on U(VI) remobilisation from those.

However, they did also mention a higher Si(IV) concentration (compared to Ca(II)) at a C/S = 0.99 after 768 h leaching with water (S/L = 1.2 g L^{-1}), which fundamentally contradicts not only this work (see Fig. 4 and Fig. S3), but also all findings from the literature (see above). A better agreement is achieved with Schmeide et al. (2025). There, the release of U(VI) due to an increase in ionic strength is considered minimal. Due to the experimental setup (batch with only one pore water cycle), they could not make any further statement regarding the retention/remobilisation mechanisms involved. Here, with the combination of the initially rapid and then again slow leaching behaviour of U(VI) in 2 M NaCl, it can be concluded that only one retention mechanism should strongly depend on the ionic strength of the electrolyte. Based on the equally strong influence on Ca(II) remobilisation, a Ca(II)-mediated U(VI) remobilisation would be obvious here. As already described in the introduction, Ca^{2+}-mediated retention mechanisms are well known in the case of C–S–H phases. Furthermore, Brix et al. (2021) described analogous Ca^{2+} bridges that contribute significantly to the retention of $UO_2(OH)_3^-$ or $UO_2(OH)_4^{2-}$ on Ca-bentonite. The fact that only relatively small amounts of U(VI) (compared to Ca(II)) are remobilised here is probably because the Ca^{2+}-mediated retention mechanism is strong but only develops to a very small extent (compared to the total retention of U(VI)). Therefore, this small proportion of bound U(VI) is only remobilised at the highest ionic strength. Together with the conclusions drawn above, coordination of $UO_2(OH)_3^-$ or $UO_2(OH)_4^{2-}$ to SiO_4 tetrahedron-bridging Ca^{2+} would therefore be conceivable. The decrease in Ca(II) leaching from 1 M NaCl to 2 M NaCl seems to contradict this working hypothesis, but as already mentioned above, it can be assumed that Ca(II) gets partially re-immobilised on formed silicate agglomerates.

Due to the experimental setup and the reproducibility shown in the experiments, combined with the agreement with the literature (in some cases), it was shown that the remobilisation of U(VI) from C–S–H phases depends (to a small extent) on the ionic strength of the electrolyte. Moreso, a possible Ca(II)-mediated retention/remobilisation mechanism dependent on ionic strength can be assumed, although this hypothesis urgently needs to be substantiated by further experiments.

3.5. Influence of Fe and Tb on leaching behaviour

To assess the influence of Fe(III) and Tb(III) as potential displacement agents, the respective leaching curves of Mo(VI), Eu(III) and U(VI) of the incorporated "WC-L_2" C–S–H phase are plotted in Fig. 6. Analogous to Chapter 3.4, the leached quantities at the end of the respective MCEs are listed in Table 6. In addition, it should also be mentioned that for Fe(III) and Tb(III) a quantitative retention of 99.9 % and >99.9 % on

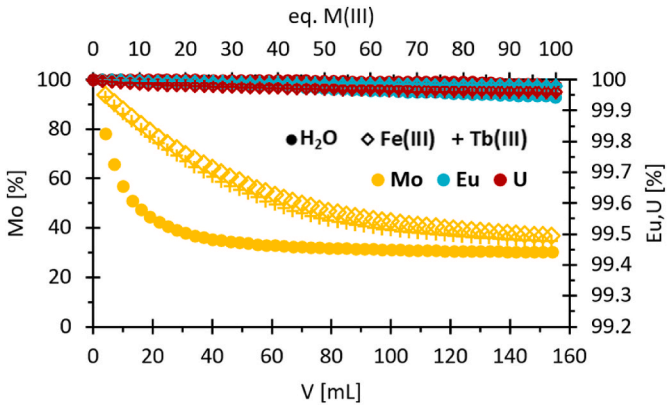

Fig. 6. Remaining Mo(VI), Eu(III) and U(VI) [%] in "WC-L_2" sample (see Table 3) plotted against pore water volume during MCE leaching experiment with and without injected displacement agent M(III) (M = Fe, Tb; equivalents in relation to incorporated Eu(III)).

Table 6
Amounts of remobilised analytes in [%] from "WC-L_2" (in relation to the values listed in Table 3) at the end of MCE leaching experiments with and without injection of different displacement agents (data from Fig. 6, S6 and S7); each after 154 mL elution volume.

Displacement agent	Leached amount [%]				
	Si	Ca	Mo	Eu	U
H_2O	9.3	14.9	69.9	0.06	0.02
Fe(III)	19.0	27.0	63.3	0.02	0.04
Tb(III)	17.2	29.1	65.3	0.02	0.04

the "WC-L_2" C–S–H phase was observed.

When comparing Tables 4 and 6 (resp. Figs. 3 and 6), no significant influence of Fe(III) or Tb(III) on the leaching behaviour of Eu(III) and U(VI) can be observed; unlike for Si(IV), Ca(II) and Mo(VI).

So far, there is no literature data for comparable displacement experiments available. Nevertheless, to create at least some basis for argumentation, the work of Schmeide et al. (2025) is used again. There, the influence of Al(III) in C-A-S-H (calcium aluminosilicate hydrate) phases on their structure and their U(VI) retention properties was systematically investigated. When Al(III) is added in the C–S–H synthesis, AlO_4-tetrahedra can form bridging positions of the silicate chains. This leads to an increase in the average chain length and creates additional sorption sites for U(VI). The increasing amount of AlO_4-tetrahedra in the bridging positions of the silicate chains in turn leads to a decrease in the C/S and an increase in the interlayer distance. In a similar study, Pardal et al. (2009) reported that Al(III) is incorporated very rapidly into the C-(A)-S-H structure, mainly by substitution of Si(IV), but also by insertion at the surface or in the interlayer of the C-(A)-S-H phases. However, also calcium carboaluminate and/or strätlingite secondary phases can be detected as soon as a Ca^{2+} concentration of >4 mmol L^{-1} was reached.

Mancini et al. (2020) published a comprehensive study on Fe(III) retention in C–S–H phases. In it, they report an extremely high retention of Fe(III) regardless of the C/S ratio and the pH of the background electrolyte. There, R_d (K_d) values of approx. 700,000 L kg^{-1} were obtained (at 5 g L^{-1}). This results in retention values of 99.97 % (according to Equation (2)), which is consistent with the results obtained here. More importantly Mancini et al. (2020) concluded from the different effects of the pH and the Ca(II) concentration, that Fe(III) in C–S–H must have a different binding mechanism, compared to Al(III). From the pH independence, they conclude that the primary Fe(III) retention mechanism is probably not based on surface complexation, and since the C/S ratio is also irrelevant, it must be the C–S–H structure per se, so that an Al(III) analogous substitution of tetrahedrally coordinated Si(IV) at the bridge position is inconceivable. Regarding the binding mechanism, it is postulated that Fe(III) coordinates octahedrally directly to the Si tetrahedra in the interlayer of the C–S–H phases at a C/S ratio between 1.2 and 1.5. At lower C/S ratios, coordination in the interlayer is rather excluded and the formation of a separate secondary Ca–Si-rich Fe(III) phase (or cluster) on the surface of C–S–H is proposed. Based on the C–S–H phases used in this work (C/S = 1.066 ± 0.003), both the formation of Ca- and Si-rich Fe(III) secondary phases and octahedral coordination in the interlayers are conceivable.

In the context of an adsorbed/incorporated lanthanide Kee et al. (2021) and Pointeau et al. (2001) have shown that Eu(III) substitutes Ca^{2+} on the cation sites. Since there are no literature references available for Tb(III) and trivalent cations share several chemical similarities, some parallels between Al(III), Fe(III), Eu(III) and Tb(III) have to be drawn here (for the time being).

Analogue to Chapter 3.4, the Si(IV) and Ca(II) leaching curves, the measured Si(IV) and Ca(II) concentrations and the measured pH are listed in the supplementary information (Figs. S5 and S6). Looking at those, as well as Table 6, a clear influence of Fe(III) and Tb(III) on the leaching behaviour of Si(IV) and Ca(II) can be observed. Especially in

Fig. S5 a significantly increased Si(IV) and Ca(II) leaching is shown when Fe(III) or Tb(III) are involved. These observations partly contradict those of Schmeide et al. (2025), who only reported a significantly increased Ca(II) concentration in solution when Al(III) is involved. The reason for this could be the different experimental setups. While they had equilibration times of >67 d at room temperature, a dynamic system (MCE) was used here. Compared to dynamic experiments, a batch only represents the beginning of a leaching curve. This means that all literature data from batch experiments are comparable with the first approx. 10 mL of the leaching curves. This results in an enormous loss of information when conducting batch experiments, and the results appear contradictory. It inevitably follows, that the data presented here must be considered more representative, and thus proving the influence of displacement agents on both Si(IV)- and Ca(II) leaching.

Based on the literature described above, the increased Si(IV) and Ca(II) release can be interpreted in a way that Fe(III) and Tb(III), similar to Al(III) and Eu(III), replace Si(IV) or Ca(II) in the C–S–H structure. In the case of Fe(III), the retention mechanism on C–S–H phases is very well described by Mancini et al. (2020) (see above). They further propose a possible substitution of Ca(II) in the interlayer by Fe(III), depending on the C/S ratio (1.2 and 1.5). Given the electron configuration and the ionic radius, for Tb(III), similar to Fe(III), an octahedral coordination is also plausible, as shown by Ananias et al. (2001) (Tb(III) in silicate solid phases). Furthermore, as already mentioned, Pointeau et al. (2001) have shown for Eu(III) and Mancini et al. (2020) for Fe(III) that Ca(II) substitution in the C–S–H phase structure have to be considered. In principle, this mechanism would also be conceivable for Tb(III). An indication for this is the decreasing C/S with increasing Al(III) content shown by literature (Schmeide et al., 2025). Assuming that SiO_4-bridging Ca^{2+} ions are also leached/substituted in the process, the amount of leached Si(IV) would increase. Based on the literature and the data presented here, this substitution mechanism appears to be the most likely cause of the increased Si(IV) and Ca(II) leaching.

In addition, a clear influence of Fe(III) and Tb(III) is also visible for Mo (VI) remobilisation. Compared to ultrapure water, the leaching is significantly delayed, whereas in the end almost the same amounts were remobilised (see Fig. 6 and Table 6). In view of the higher Ca(II) concentration, a powellite precipitation is rather unlikely, since no similar phenomena was observable with an increased ionic strength electrolyte (e.g. 1 M NaCl). At this point, a Fe(III)- and Tb(III)–MoO_4 precipitate could be possible. Based on the solubility product of $Fe_2(MoO_4)_3 \bullet 7H_2O$ ($K_{SP} = 3.16 \bullet 10^{-28}$ mol^5 L^{-5}), a possible precipitation can be estimated (Wedepohl, 1974). Considering the Eu(III) concentration listed in Table 3 and that 139.7 mg of the "WC-L_2" C–S–H phase was packed into the column, a total amount of 137.7 nmol Eu(III) can be concluded. For a 100-fold excess, 13.77 μmol Fe(III) is required, which corresponds to an Fe(III) concentration of $8.94 \bullet 10^{-5}$ mol L^{-1} (for an elution volume of 154 mL). This results in a solubility limit for Mo(VI) of $3.41 \bullet 10^{-7}$ mol L^{-1}. In both experiments, with Fe(III) and Tb(III), a Mo(VI) concentration of approx. $1.1 \bullet 10^{-6}$ mol L^{-1} was measured in the first fraction (supplementary data Fig. S7). This decreased rapidly and fell below the solubility limit after an elution volume of approx. 60 mL. Accordingly, precipitation with molybdate can therefore be expected; at least for Fe(III). For Tb(III) there is unfortunately no literature data regarding the solubility product, but rare earth-/lanthanide-molybdates are often used as phosphors, optical fibres, scintillators, laser hosts and are therefore well-known to literature (Brixner et al., 1979; Huang et al., 1989; Pourmortazavi et al., 2019). One possible synthesis route is the direct precipitation reaction in an aqueous environment, as described, for example, by Pourmortazavi et al. (2019). This can be associated with a low solubility product and therefore, with the formation of $Tb_2(MoO_4)_3$ during the leaching experiments. Furthermore, considering the data shown in Fig. 6, Fig. S7 and Table 6 a similar but slightly weaker effect on the Mo(VI) remobilisation can be seen. This could be interpreted as an indication of a just slightly higher K_{SP} of $Tb_2(MoO_4)_3$ (compared to the Fe(III) analogue). Another possible explanation for the delayed Mo(VI) remobilisation could be found in the results reported by (Mancini et al., 2020). As described above, the formation of Fe(III) secondary phases was reported, which in turn could provide new potential sorption sites for Mo(VI). If this assumption is correct, then the same should also apply to Tb(III). However, this leaves one question open: Why do the postulated, already existing Eu(III) secondary phases formed during C–S–H synthesis do not exhibit a comparable effect? Further extensive spectroscopic investigations may help to clarify the dynamics of Mo(VI) remobilisation.

Regarding the lack of influence of Fe(III) and Tb(III) on Eu(III) and U(VI) retention, it is difficult to determine at this point whether: 1) Eu(III) and U(VI) were incorporated "too deep" into the C–S–H structure during synthesis and are therefore not accessible to Fe(III) and Tb(III); 2) Eu(III) and U(VI) occupied other binding sites than Fe(III) and Tb(III); or 3) the binding of Eu(III) and U(VI) is significantly stronger than that of Fe(III) and Tb(III). Point 1) is contradicted by the fact that, for example, ion strength (see above) and PBTC (see below) can influence the remobilisation of Eu(III) or U(VI). This indicates that they should be sensitive to post-synthesis perturbation. Points 2) and 3) are therefore much more likely. In the case of Eu(III), which has itself substituted Ca^{2+} in the interlayers, point 3) seems most likely, which in turn implies that Fe(III) and Tb(III) are not able to displace it. In the case of U(VI), point 2) seems more likely. However, an accurate assessment is not possible at this point, so further investigations are advisable, ideally supplemented by geochemical modelling.

3.6. *Influence of PBTC on leaching behaviour*

Finally, the influence of PBTC on the leaching behaviour will be discussed. For this purpose, Fig. 7 shows the leaching curves of Mo(VI), Eu(III) and U(VI) under the influence of PBTC. The corresponding concentrations are shown in the supplementary data (Fig. S10). In addition, Table 7 shows the leached relative quantities without, after a 500-fold and after a 1000-fold excess of PBTC; as already mentioned, the excess refers to the initially bound quantity of Eu(III).

Looking first at the leaching of Si(IV) and Ca(II) (Figs. S8 and S9 and Table 7), a clear influence of PBTC can be seen. In the case of Ca(II), up to approx. 30 mL elution volume, less Ca(II) is initially leached compared to ultrapure water (see Fig. S8), whereas considerably more is leached afterwards. In the case of Si(IV) during the whole experiment more Si(IV) is leached with PBTC, than in ultrapure water. However, most interesting in Fig. S8 is the sharp drop in the leached Si(IV) and Ca(II) amount at 180 mL elution volume (600 eq. PBTC). As PBTC is an acid, pH influences are conceivable, but, as Fig. S8 shows, this behaves analogously to the experiments in ultrapure water. Only a very small step is visible at approx. 170 mL. Therefore, only the interaction of PBTC with the analytes themselves is relevant. According to Kretzschmar et al.

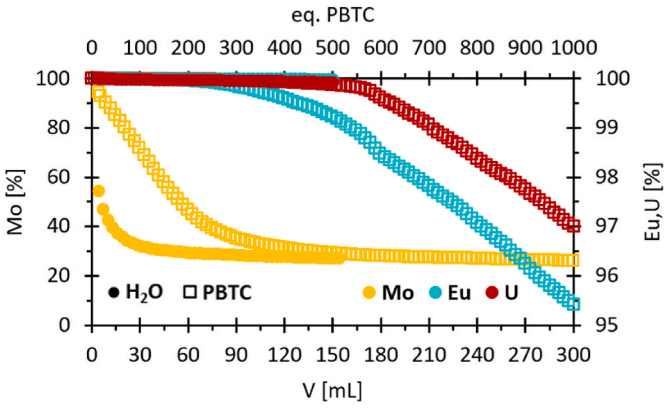

Fig. 7. Remaining Mo(VI), Eu(III) and U(VI) [%] in "WC-L_1" sample (see Table 3) plotted against pore water volume during MCE leaching experiment with and without PBTC (in relation to incorporated Eu(III)) injected; without PBTC (dots) same data as shown in Fig. 5.

Table 7
Amounts of remobilised analytes in [%] (in relation to the values listed in Table 3) from "WC L_1" in MCE leaching experiments after the injection of different amounts of PBTC (Data from Fig. 7, S9 and S10); without PBTC same data as shown in Tables 4 and 5; 500-fold excess refers to data in Fig. 7 after 154 mL/500 eq. PBTC; 1000-fold excess refers to data in Fig. 7 after 304 mL/1000 eq. PBTC.

Excess of PBTC (eq. Eu)	Leached amount [%]				
	Si	Ca	Mo	Eu	U
–	8.5	17.1	72.9	0.015	0.076
500	13.9	20.7	71.0	0.807	0.131
1000	20.3	26.3	73.8	4.58	3.00

(2022), at a pH = 10, PBTC is present as a 50/50 mixture of the 4-fold (HL^{4-}) and 5-fold (L^{5-}) deprotonated ligand. From a pH > 11, however, the L^{5-} species dominates (>95 %). Thus, in the measured pH range, many multidentate/chelate complexation reactions with the analytes are conceivable. In addition to the strong complexing properties of PBTC for a variety of metals, basic interactions of PBTC with cement phases, including C–S–H, are also known (Salvadó et al., 1999; Rickert and Thielen, 2004; Spinthaki et al., 2018; Huang et al., 2020). Regarding the incorporated elements, the work of Huang et al. (2020) is very interesting. They functionalised nanoparticles with PBTC and investigated their capacity for a variety of metal ions (including U(VI) and Eu(III)). Under acidic conditions (pH = 4) a capacity of up to 99 mg g^{-1} ($4.16 \bullet 10^{-4}$ mol g^{-1}) was measured for U(VI) and up to 41 mg g^{-1} ($2.70 \bullet 10^{-4}$ mol g^{-1}) for Eu(III). However, the higher affinity towards U (VI) should not be given too much importance, as the pH range is completely different from the one here and thus, due to changed speciation the affinity could shift in favour of Eu(III). In the case of the C–S–H-PBTC interactions, Rickert and Thielen (2004) report that PBTC either: 1) partially adsorbs on the C–S–H phases surface; 2) complexes Ca(II) ions; 3) precipitates as a sparingly soluble Ca phosphonate ($Ca_{2.5}[C_7H_6O_9P] \bullet xH_2O$), which then partially adsorbs on the C–S–H surface, when a certain Ca(II) concentration is reached.

Based on this, the results in Fig. S8 can be interpreted in such a way that PBTC leads to a generally increased C–S–H leaching, whereby the amount of Ca(II) leached exceeds the threshold (not defined in more detail by Rickert and Thielen (2004)) and partly precipitates as $Ca_{2.5}[C_7H_6O_9P] \bullet xH_2O$. In the case of Si(IV), the threshold defined in Chapter 3.4 seems not to be reached, whereby Si(IV) is not agglomerated/re-retained and is therefore fully remobilised (see Figs. S3 and S8). Based on the data currently available, it is difficult to make a reliable statement about the underlying phenomena for the breakdown of remobilisation at 180 mL (Fig. S8). A possible solution is again offered by Rickert and Thielen (2004). They describe that the $Ca_{2.5}[C_7H_6O_9P] \bullet xH_2O$ precipitate adsorbed on the surface can form a coating, whereby the C–S–H solid phase is completely enclosed. In that case, the C–S–H phase would no longer be accessible to PBTC, and leaching would consequently collapse.

The hypothesis of the Ca-phosphonate coat is also supported by the U (VI) leaching curve (Fig. 7 and S10). From the point at which C–S–H leaching decreases abruptly, that of U(VI) increases rapidly. At this tipping point, less Ca(II) is available for the formation of possible Ca(II)-PBTC precipitates or complexes, which in turn would lead to more PBTC being available in solution. Due to this shift in equilibrium, U(VI) would now also be complexed and remobilised. However, it must be noted that only the dissolution of a U(VI) secondary phases would be possible at this point, as the C–S–H phases, as described above, are no longer accessible.

In the case of Mo(VI) and Eu(III), the data are again not easy to explain but also support the hypothesis of the Ln(III)-molybdate secondary phase (see Chapter 3.5). As can be seen from Fig. 7 and Fig. S10, the Mo(VI) leaching is significantly slower when PBTC is involved; quite similar to the effect of Fe(III) and Tb(III). If PBTC remobilises bound Eu(III) (or from secondary phases), this free or complexed Eu(III) could then precipitate with Mo(VI) as $Eu_2(MoO_4)_3$. In this case, however, the precipitation as molybdate must be clearly preferential compared to the Eu(III)-PBTC complex. Assuming all this, the increased Eu(III) concentration in Fig. S10 and with that the increasing Eu(III) leaching (Fig. 7) is also well explained, since Eu(III) concentration/remobilisation rises significantly as soon as the one of Mo(VI) drops. Another possible reason for the leaching curves of Mo(VI), and Eu(III), could be delivered by the precipitation of $Ca_{2.5}[C_7H_6O_9P] \bullet xH_2O$. In that case, a Mo(VI)–Ca(II)-phosphonate-coprecipitate would be suspected and for Eu(III) the same applies as for U(VI): The Ca(II)-phosphonate (or a Mo(VI)–Ca(II)-phosphonate) coat inhibits the accessibility of C–S–H for PBTC, less Ca(II) is available for possible Ca(II)-PBTC precipitates or complexes, more PBTC is available in solution and Eu(III) is now complexed and remobilised. The difference here is, that, compared to U(VI), a stronger PBTC complex have to be formed, since Eu(III) leaching starts earlier (see Fig. 7 and Fig. S10).

The conclusions drawn here should be regarded as preliminary and cannot be fully substantiated based on the data currently available. Here too, additional investigations in combination with geochemical modelling are advisable.

4. Conclusion

In this study, C–S–H phases containing trace amounts of the repository-relevant elements Mo(VI), Eu(III) and U(VI) were synthesised and characterised. An elemental analysis of the supernatant solutions confirmed a successful incorporation of all three elements into the C–S–H phase. X-ray diffractometry showed that the synthesis was successful, and no noticeable impact of the elements added on the C–S–H phases' structure could be identified. ICP-QQQ analysis had shown, that the synthesised C–S–H phases had a C/S ratio of 1.066 ± 0.003.

The reproducible results derived from standardized batch experiments and MCE with ultrapure water confirmed the expected leaching behaviour for Si(IV) and Ca(II); initially more calcium-followed by coherent leaching. In the case of europium and uranium, in both setups (batch and MCE) quantitative retention was observed, confirming earlier results in the literature. Molybdenum, on the other hand, was remobilised after only a few pore water exchange cycles, although not completely. Two different mechanisms are postulated here: weakly bound adsorption on/in the C–S–H structure and precipitation of $CaMoO_4$. These mechanisms had been suspected before, but this is the first time that the hypothesis of both mechanisms has been substantiated with experimental data. In general, the setups showed clear differences. Here, leaching/remobilisation was supposedly stronger pronounced in the batch than in the MCE setup, which can be explained primarily by the state of equilibration and the S/L ratio.

Since MCE are more representative for the conditions in a HLW repository, they were the baseline approach for all further studies. An increase in ionic strength of up to 1 M enhanced both Ca(II) and Si(IV) leaching. At an ionic strength of I = 2 M, a decrease in leaching for both elements were observed, possibly due to the formation of silicate agglomerates on which calcium could adsorb. This supposed mechanism requires further confirmation by future investigations. A higher ionic strength did not notably impact the remobilisation of Eu(III) and Mo(IV). However, contrary to some literature reports, a slight but significant increase in U(VI) remobilisation at I = 2 M could be demonstrated. The cause is postulated to be the release of a Ca(II) mediated U(VI) retention mechanism. This is especially relevant since in HLW repositories, depending on their geochemical conditions, porewaters with high ionic strength of up to I = 5 M can be expected. Additional studies with background electrolytes at such ionic strength are therefore recommended.

The addition of the competitive ions Fe(III) and Tb(III) as displacement agents had no influence on the remobilisation dynamics of Eu(III) and U(VI). However, an increase in the Si(IV) and Ca(II) leaching was

observed. Based on those results and the literature available, a substitution of the structure-forming Ca^{2+} ions in the C–S–H phase is suggested. More importantly, the displacement agents delayed and retarded the remobilisation of Mo(VI), which is why the precipitation of insoluble trivalent metal molybdates is proposed.

PBTC as a potential cement additive and complexing agent enhances the leaching of Si(IV), Ca(II), Eu(III) and U(VI), whereas that of Mo(VI) is slightly retarded. During complexation, further interaction mechanisms are also induced. For example, a proposed calcium phosphonate precipitate coating leads to a delayed but rapid U(VI) remobilisation. Furthermore, an earlier remobilisation was observed for Eu(III) compared to U(VI), indicating a preferential complexation of europium. In the case of retarded Mo(VI) remobilisation, co-precipitation molybdenum calcium phosphonates is postulated as a possible reason. However, further studies with appropriate methods to make definite statements are required to confirm the mechanisms of the remobilisation in presence of PBTC.

In summary, this study provides important insights into the retention and dynamic remobilisation of molybdenum, europium, and uranium on C–S–H phases (C/S $\approx$ 1). While it closes critical knowledge gaps and confirms existing hypotheses, it also challenges others. Although currently limited to a single C/S ratio, this work establishes a vital foundation for future geochemical modelling and experimental research, moving us closer to a comprehensive mechanistic understanding of the investigated repository-relevant systems.

CRediT authorship contribution statement

Aaron Haben: Writing – review & editing, Writing – original draft, Visualization, Validation, Methodology, Investigation, Formal analysis, Data curation, Conceptualization. **Nico Bachmann:** Writing – review & editing, Validation, Investigation, Formal analysis, Data curation, Methodology, Visualization. **Jan Jakob Langer:** Writing – review & editing, Writing – original draft, Validation. **Ralf Kautenburger:** Writing – review & editing, Validation, Supervision, Project administration, Funding acquisition, Conceptualization.

Declaration of generative AI and AI-assisted technologies in the writing process generative-ai

During the preparation of this work the authors used DeepL to help with the translation and wording of some passages. After using this tool/service, the authors reviewed and edited the content as needed and take full responsibility for the content of the publication.

Declaration of competing interest

The authors declare that they have no known competing financial interests or personal relationships that could have appeared to influence the work reported in this paper.

Acknowledgements

This work was supported by the German Federal Ministry for the Environment, Nature Conservation, Nuclear Safety and Consumer Protection (BMUV), represented by the Project Management Agency Karlsruhe (PTKA-WTE) [grant number 02E11860D]. ICP-QQQ instrumentation for this work was financially supported from Saarland University and German Research Foundation [project number INST 256/553-1]. We would like to thank our project partners for the kind collaboration and Anna Jennewein for the assistance with the Graphical Abstract. XRD instrumentation and technical assistance for this work was provided by the Service Center X-ray Diffraction, with financial support from Saarland University and German Research Foundation [project number INST 256/349-1]. The authors thank Anna Michaely for the support in collection of the X-ray diffraction data presented in this paper.

Appendix A. Supplementary data

Supplementary data to this article can be found online at https://doi.org/10.1016/j.apgeochem.2026.106684.

Data availability

Data will be made available on request.

References

Ananias, D., Ferreira, A., Rocha, J., Ferreira, P., Rainho, J.P., Morais, C., Carlos, L.D., 2001. Novel microporous Europium and terbium silicates. J. Am. Chem. Soc. 123, 5735–5742. https://doi.org/10.1021/ja010244z.

Androniuk, I., Kalinichev, A.G., 2020. Molecular dynamics simulation of the interaction of uranium (VI) with the C-S-H phase of cement in the presence of gluconate. Appl. Geochem. 113, 104496. https://doi.org/10.1016/j.apgeochem.2019.104496.

Androniuk, I., Landesman, C., Henocq, P., Kalinichev, A.G., 2017. Adsorption of gluconate and uranyl on C-S-H phases: combination of wet chemistry experiments and molecular dynamics simulations for the binary systems. Phys. Chem. Earth 99, 194–203. https://doi.org/10.1016/j.pce.2017.05.005.

Atkins, M., Glasser, F.P., Kindness, A., 1992. Cement hydrate phase: solubility at 25°C. Cement Concr. Res. 22, 241–246. https://doi.org/10.1016/0008-8846(92)90062-Z.

Baqer, Y., Thornton, S., Stewart, D.I., Norris, S., Chen, X., 2023. Analysis of uranium sorption in a laboratory column experiment using a reactive transport and surface complexation model. Transport Porous Media 149, 423–452. https://doi.org/10.1007/s11242-023-01956-y.

Baston, G.M.N., Clacher, A.P., Heath, T.G., Hunter, F.M.I., Smith, V., Swanton, S.W., 2012. Calcium silicate hydrate (C-S-H) gel dissolution and pH buffering in a cementitious near field. Mineral. Mag. 76, 3045–3053. https://doi.org/10.1180/minmag.2012.076.8.20.

Baur, S., Brix, K., Feuerstein, A., Janka, O., Kautenburger, R., 2022. Retention of waste cocktail elements onto characterised calcium silicate hydrate (C-S-H) phases: a kinetic study under highly saline and hyperalkaline conditions. Appl. Geochem. 143, 105319. https://doi.org/10.1016/j.apgeochem.2022.105319.

Brix, K., Baur, S., Haben, A., Kautenburger, R., 2021. Building the bridge between U(VI) and Ca-bentonite – influence of concentration, ionic strength, pH, clay composition and competing ions. Chemosphere 285, 131445. https://doi.org/10.1016/j.chemosphere.2021.131445.

Brix, K., Haben, A., Kautenburger, R., 2023. Time-dependent retention of a mixture of Cs (I), Sm(III), Eu(III) and U(VI) as waste cocktail by calcium silicate hydrate (C-S-H) phases. Minerals 13, 1469. https://doi.org/10.3390/min13121469.

Brixner, L.H., Barkley, J.R., Jeitschko, W., 1979. Chapter 30 rare Earth molybdates (VI). Handbook on the Physics and Chemistry of Rare Earths. Elsevier 609–654. https://doi.org/10.1016/S0168-1273(79)03013-0.

Burešová, M., Kittnerová, J., Drtinová, B., 2023. Comparative study of Eu and U sorption on cementitious materials in the presence of organic substances. J. Radioanal. Nucl. Chem. 332, 1499–1504. https://doi.org/10.1007/s10967-022-08705-3.

Burger, E., Rebiscoul, D., Bruguier, F., Jublot, M., Lartigue, J.E., Gin, S., 2013. Impact of iron on nuclear glass alteration in geological repository conditions: a multiscale approach. Appl. Geochem. 31, 159–170. https://doi.org/10.1016/j.apgeochem.2012.12.016.

Caselles, L.D., Roosz, C., Hot, J., Blotevogel, S., Cyr, M., 2021. Immobilization of molybdenum by alternative cementitious binders and synthetic C-S-H: an experimental and numerical study. Sci. Total Environ. 789, 148069. https://doi.org/10.1016/j.scitotenv.2021.148069.

Cotton, S., 2006. Lanthanide and Actinide Chemistry. Wiley. https://doi.org/10.1002/0470010088.

Cross, J.N., Macor, J.A., Bertke, J.A., Ferrier, M.G., Girolami, G.S., Kozimor, S.A., Maassen, J.R., Scott, B.L., Shuh, D.K., Stein, B.W., Stieber, S.C.E., 2016. Comparing the 2,2′-Biphenylenedithiophosphinate binding of americium with neodymium and Europium. Angew. Chem. 128, 12947–12951. https://doi.org/10.1002/ange.201606367.

Dettmann, S., Huittinen, N.M., Jahn, N., Kretzschmar, J., Kumke, M.U., Kutyma, T., Lohmann, J., Reich, T., Schmeide, K., Shams Aldin Azzam, S., Spittler, L., Stietz, J., 2023. Influence of gluconate on the retention of Eu(III), Am(III), Th(IV), Pu(IV), and U(VI) by C-S-H (C/S = 0.8). Front. Nucl. Eng. 2. https://doi.org/10.3389/fnuen.2023.1124856.

Dörr, S., Bollingerfehr, W., Filbert, W., Tholen, M., 2013. Quantity and management of spent fuel from prototype and research reactors in Germany. Proceedings of the ASME 2013 15th International Conference on Environmental Remediation and Radioactive Waste Management. https://doi.org/10.1115/ICEM2013-96040.

Efremenkov, V., Drace, Z., 2007. Considerations for Waste Minimization at the Design Stage of Nuclear Facilities. IAEA, Vienna. STI/DOC/010/460.

Eisenbud, M., Krauskopf, K., Franca, E.P., Lei, W., Ballad, R., Linsalata, P., Fujimori, K., 1984. Natural analogues for the transuranic actinide elements: an investigation in Minas Gerais, Brazil. Environ. Geol. Water Sci. 6, 1–9. https://doi.org/10.1007/BF02525564.

Essington, M.E., 1990. Calcium molybdate solubility in spent oil shale and a preliminary evaluation of the association constants for the formation of $CaMoO_4^0$(aq),

KMoO$_4^-$(aq), and NaMoO$_4^-$(aq). Environ. Sci. Technol. 24, 214–220. https://doi.org/10.1021/es00072a010.
Evans, N.D.M., 2008. Binding mechanisms of radionuclides to cement. Cement Concr. Res. 38, 543–553. https://doi.org/10.1016/j.cemconres.2007.11.004.
Feng, M., Qiu, J., Zhou, X., Wang, L., Li, T., Xie, J., Yang, M., 2024. Influence of flow on the corrosion behavior of pure iron in simulated geological repository conditions. Surf. Interfaces 46, 103998. https://doi.org/10.1016/j.surfin.2024.103998.
Féron, D., Crusset, D., Gras, J.-M., 2008. Corrosion issues in nuclear waste disposal. J. Nucl. Mater. 379, 16–23. https://doi.org/10.1016/j.jnucmat.2008.06.023.
Freiesleben, H., 2013. Final disposal of radioactive waste. EPJ Web Conf. 54. https://doi.org/10.1051/epjconf/20135401006.
Gaona, X., Dähn, R., Tits, J., Scheinost, A.C., Wieland, E., 2011. Uptake of Np(IV) by C-S-H phases and cement paste: an EXAFS study. Environ. Sci. Technol. 45, 8765–8771. https://doi.org/10.1021/es2012897.
Glasser, F.P., Pedersen, J., Goldthorpe, K., Atkins, M., 2005. Solubility reactions of cement components with NaCl solutions: I. Ca(OH)$_2$ and C-S-H. Adv. Cement Res. 17, 57–64. https://doi.org/10.1680/adcr.2005.17.2.57.
Goo, J.-Y., Kim, B.-J., Kang, M., Jeong, J., Jo, H.Y., Kwon, J.-S., 2021. Leaching behavior of cesium, strontium, cobalt, and Europium from immobilized cement matrix. Appl. Sci. 11, 8418. https://doi.org/10.3390/app11188418.
Grambow, B., López-García, M., Olmeda, J., Grivé, M., Marty, N.C.M., Grangeon, S., Claret, F., Lange, S., Deissmann, G., Klinkenberg, M., Bosbach, D., Bucur, C., Florea, I., Dobrin, R., Isaacs, M., Read, D., Kittnerová, J., Drtinová, B., Vopálka, D., Cevirim-Papaioannou, N., Ait-Mouheb, N., Gaona, X., Altmaier, M., Nedyalkova, L., Lothenbach, B., Tits, J., Landesman, C., Rasamimanana, S., Ribet, S., 2020. Retention and diffusion of radioactive and toxic species on cementitious systems: main outcome of the CEBAMA project. Appl. Geochem. 112, 104480. https://doi.org/10.1016/j.apgeochem.2019.104480.
Grangeon, S., Claret, F., Linard, Y., Chiaberge, C., 2013. X-ray diffraction: a powerful tool to probe and understand the structure of nanocrystalline calcium silicate hydrates. Acta Crystallogr. B 69, 465–473. https://doi.org/10.1107/S2052519213021155.
Grangeon, S., Claret, F., Roosz, C., Sato, T., Gaboreau, S., Linard, Y., 2016. Structure of nanocrystalline calcium silicate hydrates: insights from X-ray diffraction, synchrotron X-ray absorption and nuclear magnetic resonance. J. Appl. Crystallogr. 49, 771–783. https://doi.org/10.1107/S1600576716003885.
Haben, A., Brix, K., Bachmann, N., Kautenburger, R., 2024. Sorption experiments as efficient as possible: Mini-Column experiments (MCE) using HPLC-ICP-MS coupling with a new data analysis approach to determine sorption parameters. Microchem. J. 206, 111511. https://doi.org/10.1016/j.microc.2024.111511.
Harfouche, M., Wieland, E., Dähn, R., Fujita, T., Tits, J., Kunz, D., Tsukamoto, M., 2006. EXAFS study of U(VI) uptake by calcium silicate hydrates. J. Colloid Interface Sci. 303, 195–204. https://doi.org/10.1016/j.jcis.2006.07.019.
Hege, N., Poore, A.T., Galley, S.S., Reinhart, B.J., Jackson, J.A., Tian, S., Shafer, J.C., 2024. Understanding europium and terbium speciation and ion pairing in carbonate complexes using advanced spectroscopy techniques. Eur. J. Inorg. Chem. 27, e202400011. https://doi.org/10.1002/ejic.202400011.
Hill, J., Harris, A.W., Manning, M., Chambers, A., Swanton, S.W., 2006. The effect of sodium chloride on the dissolution of calcium silicate hydrate gels. Waste Manage. (Tucson, Ariz.) 26, 758–768. https://doi.org/10.1016/j.wasman.2006.01.022.
Huang, Q., Xu, J.-Z., Li, W., 1989. Preparation of tetragonal defect scheelite-type RE$_2$(MoO$_4$)$_3$ (RE=La TO Ho) by precipitation method. Solid State Ionics 32–33, 244–249. https://doi.org/10.1016/0167-2738(89)90228-2.
Huang, Y., Zheng, H., Li, H., Zhao, C., Zhao, R., Li, S., 2020. Highly selective uranium adsorption on 2-phosphonobutane-1,2,4-tricarboxylic acid-decorated chitosan-coated magnetic silica nanoparticles. Chem. Eng. J. 388, 124349. https://doi.org/10.1016/j.cej.2020.124349.
Jacques, D., Wang, L., Martens, E., Mallants, D., 2009. Time Dependence of the Geochemical Boundary Conditions for the Cementitious Engineered Barriers of the Belgian Surface Disposal Facility - Project near Surface Disposal of Category A Waste at Dessel. ONDRAF/NIRAS, Brussel, Belgium, NIROND-TR 2008-24E.
Jobmann, M., Bebiolka, A., Burlaka, V., Herold, P., Jahn, S., Lommerzheim, A., Maßmann, J., Meleshyn, A., Mrugalla, S., Reinhold, K., Rübel, A., Stark, L., Ziefle, G., 2017. Safety assessment methodology for a German high-level waste repository in clay formations. J. Rock Mech. Geotech. Eng. 9, 856–876. https://doi.org/10.1016/j.jrmge.2017.05.007.
Kautenburger, R., Beck, H.P., 2008. Waste disposal in clay formations: influence of Humic acid on the migration of heavy-metal pollutants. ChemSusChem 1, 295–297. https://doi.org/10.1002/cssc.200800014.
Kee, C.C., Ang, B.C., Metselaar, H.S.C., 2021. Synthesis of europium-doped calcium silicate hydrate via hydrothermal and coprecipitation method. Ceram. Int. 47, 4803–4812. https://doi.org/10.1016/j.ceramint.2020.10.050.
Krauskopf, K.B., 1986. Thorium and rare-earth metals as analogs for actinide elements. Chem. Geol. 55, 323–335. https://doi.org/10.1016/0009-2541(86)90033-1.
Kretzschmar, J., Wollenberg, A., Tsushima, S., Schmeide, K., Acker, M., 2022. 2-Phosphonobutane-1,2,4,-Tricarboxylic acid (PBTC): pH-Dependent behavior studied by means of multinuclear NMR spectroscopy. Molecules 27, 4067.
Lange, S., Klinkenberg, M., Barthel, J., Bosbach, D., Deissmann, G., 2020. Uptake and retention of molybdenum in cementitious systems. Appl. Geochem. 119, 104630. https://doi.org/10.1016/j.apgeochem.2020.104630.
Li, M.-H., Wang, T.-H., Teng, S.-P., 2009. Experimental and numerical investigations of effect of column length on retardation factor determination: a case study of cesium transport in crushed granite. J. Hazard. Mater. 162, 530–535. https://doi.org/10.1016/j.jhazmat.2008.05.076.
Lommerzheim, A., Jobmann, M., Meleshyn, A., Mrugalla, S., Rübel, A., Stark, L., 2019. Safety concept, FEP catalogue and scenario development as fundamentals of a long-term safety demonstration for high-level waste repositories in German clay formations. Geol. Soc. Spec. Publ. 482, 313–329. https://doi.org/10.1144/SP482.6.
Lothenbach, B., Nonat, A., 2015. Calcium silicate hydrates: solid and liquid phase composition. Cement Concr. Res. 78, 57–70. https://doi.org/10.1016/j.cemconres.2015.03.019.
Luhar, I., Luhar, S., Abdullah, M.M.A.B., Sandu, A.V., Vizureanu, P., Razak, R.A., Burduhos-Nergis, D.D., Imjai, T., 2023. Solidification/Stabilization technology for radioactive wastes using cement: an appraisal. Materials 16, 954.
Macé, N., Page, J., Reiller, P.E., 2023. Uranium(VI) sorption onto hardened cement paste under high saline and alkaline conditions. Minerals 13. https://doi.org/10.3390/min13030325.
Macé, N., Wieland, E., Dähn, R., Tits, J., Scheinost, A.C., 2013. EXAFS investigation on U (VI) immobilization in hardened cement paste: influence of experimental conditions on speciation. Radiochim. Acta 101, 379–389. https://doi.org/10.1524/ract.2013.2024.
Mancini, A., Wieland, E., Geng, G., Dähn, R., Skibsted, J., Wehrli, B., Lothenbach, B., 2020. Fe(III) uptake by calcium silicate hydrates. Appl. Geochem. 113, 104460. https://doi.org/10.1016/j.apgeochem.2019.104460.
Mandaliev, P., Stumpf, T., Tits, J., Dähn, R., Walther, C., Wieland, E., 2011. Uptake of Eu (III) by 11Å tobermorite and xonotlite: a TRLFS and EXAFS study. Geochem. Cosmochim. Acta 75, 2017–2029. https://doi.org/10.1016/j.gca.2010.10.028.
Maragkou, E., Pashalidis, I., 2022. The effect of EDTA on the desorption of uranium from calcium silicate hydrate matrices. J. Radioanal. Nucl. Chem. 331, 507–510. https://doi.org/10.1007/s10967-021-08089-w.
Motta, A.T., Couet, A., Comstock, R.J., 2015. Corrosion of zirconium alloys used for nuclear fuel cladding. Annu. Rev. Mater. Res. 45, 311–343. https://doi.org/10.1146/annurev-matsci-070214-020951.
Ochs, M., Mallants, D., Wang, L., 2016. Radionuclide and metal sorption on cement and concrete. Topics in Safety, Risk, Reliability and Quality. Springer. https://doi.org/10.1007/978-3-319-23651-3.
Oelkers, E.H., Montel, J.-M., 2008. Phosphates and nuclear waste storage. Elements 4, 113–116. https://doi.org/10.2113/gselements.4.2.113.
Papatzani, S., Paine, K., Calabria-Holley, J., 2015. A comprehensive review of the models on the nanostructure of calcium silicate hydrates. Constr. Build. Mater. 74, 219–234. https://doi.org/10.1016/j.conbuildmat.2014.10.029.
Pardal, X., Pochard, I., Nonat, A., 2009. Experimental study of Si–Al substitution in calcium-silicate-hydrate (C-S-H) prepared under equilibrium conditions. Cement Concr. Res. 39, 637–643. https://doi.org/10.1016/j.cemconres.2009.05.001.
Pointeau, I., Landesman, C., Giffaut, E., Reiller, P., 2004. Reproducibility of the uptake of U(VI) onto degraded cement pastes and calcium silicate hydrate phases. Radiochim. Acta 92, 645–650. https://doi.org/10.1524/ract.92.9.645.55008.
Pointeau, I., Piriou, B., Fedoroff, M., Barthes, M.G., Marmier, N., Fromage, F., 2001. Sorption mechanisms of Eu^{3+} on CSH phases of hydrated cements. J. Colloid Interface Sci. 236, 252–259. https://doi.org/10.1006/jcis.2000.7411.
Pourmortazavi, S.M., Rahimi-Nasrabadi, M., Aghazadeh, M., Karimi, M.S., Ganjali, M.R., Norouzi, P., 2019. Optimizing the synthesis of terbium(III) molybdate nanoplates through an orthogonal array design. Environ. Prog. Sustain. Energy 38, 13091. https://doi.org/10.1002/ep.13091.
Richardson, I.G., 2008. The calcium silicate hydrates. Cement Concr. Res. 38, 137–158. https://doi.org/10.1016/j.cemconres.2007.11.005.
Rickert, J., Thielen, G., 2004. Influence of a long-term retarder on the hydration of clinker and cement. Cem. Concr. Aggregates 26, 1–10. https://doi.org/10.1520/cca12315.
Salvadó, V., Escoda, M.L.s., de la Torre, F., 1999. A study of the complex formation between trivalent ions (Al^{3+}, Fe^{3+}) and 2-phosphonobutane-1,2,4-tricarboxylic acid and their industrial applications. Polyhedron 18, 3275–3280. https://doi.org/10.1016/S0277-5387(99)00264-8.
Schmeide, K., Huittinen, N.M., Shams Aldin Azzam, S., Bok, F., Brendler, E., Lothenbach, B., Kretzschmar, J., 2025. Uranium(VI) retention by calcium (alumino) silicate hydrates – impact of temperature and ionic strength. Appl. Geochem. 186, 106400. https://doi.org/10.1016/j.apgeochem.2025.106400.
Shrestha, R., Černoušek, T., Stoulil, J., Kovářová, H., Sihelská, K., Špánek, R., Ševců, A., Steinová, J., 2021. Anaerobic microbial corrosion of carbon steel under conditions relevant for deep geological repository of nuclear waste. Sci. Total Environ. 800, 149539. https://doi.org/10.1016/j.scitotenv.2021.149539.
Spence, R.D., 1993. Chemistry and Microstructure of Solidified Waste Forms. Lewis Publishers, Boca Raton.
Spinthaki, A., Matheis, J., Hater, W., Demadis, K.D., 2018. Antiscalant-Driven inhibition and stabilization of "Magnesium Silicate" under geothermal stresses: the role of magnesium–phosphonate coordination chemistry. Energy Fuel. 32, 11749–11760. https://doi.org/10.1021/acs.energyfuels.8b02704.
Sugiyama, D., 2008. Chemical alteration of calcium silicate hydrate (C–S–H) in sodium chloride solution. Cement Concr. Res. 38, 1270–1275. https://doi.org/10.1016/j.cemconres.2008.06.002.
Tits, J., Fujita, T., Tsukamoto, M., Wieland, E., 2008. Uranium(VI) uptake by synthetic calcium Silicate hydrates. MRS Online Proc. Libr. 1107, 467. https://doi.org/10.1557/PROC-1107-467.
Tits, J., Geipel, G., Macé, N., Eilzer, M., Wieland, E., 2011. Determination of uranium(VI) sorbed species in calcium silicate hydrate phases: a laser-induced luminescence spectroscopy and batch sorption study. J. Colloid Interface Sci. 359, 248–256. https://doi.org/10.1016/j.jcis.2011.03.046.
Tits, J., Stumpf, T., Rabung, T., Wieland, E., Fanghänel, T., 2003. Uptake of Cm(III) and Eu(III) by calcium Silicate hydrates: a solution chemistry and time-resolved laser Fluorescence spectroscopy study. Environ. Sci. Technol. 37, 3568–3573. https://doi.org/10.1021/es030020b.

Tits, J., Walther, C., Stumpf, T., Macé, N., Wieland, E., 2015. A luminescence line-narrowing spectroscopic study of the uranium(vi) interaction with cementitious materials and titanium dioxide. Dalton Trans. 44, 966–976. https://doi.org/10.1039/C4DT02172J.

Tits, J., Wieland, E., Müller, C.J., Landesman, C., Bradbury, M.H., 2006. Strontium binding by calcium silicate hydrates. J. Colloid Interface Sci. 300, 78–87. https://doi.org/10.1016/j.jcis.2006.03.043.

Walker, C.S., Sutou, S., Oda, C., Mihara, M., Honda, A., 2016. Calcium silicate hydrate (C-S-H) gel solubility data and a discrete solid phase model at 25°C based on two binary non-ideal solid solutions. Cement Concr. Res. 79, 1–30. https://doi.org/10.1016/j.cemconres.2015.07.006.

Wang, T.-H., Li, M.-H., Teng, S.-P., 2009. Bridging the gap between batch and column experiments: a case study of Cs adsorption on granite. J. Hazard. Mater. 161, 409–415. https://doi.org/10.1016/j.jhazmat.2008.03.112.

Wedepohl, K.H., 1974. Elements Kr (36) to Ba (56), Handbook of Geochemistry. Springer, Berlin.

Welch, J.M., Müller, D., Knoll, C., Wilkovitsch, M., Giester, G., Ofner, J., Lendl, B., Weinberger, P., Steinhauser, G., 2017. Picomolar traces of Americium(III) introduce drastic changes in the structural chemistry of Terbium(III): a break in the "Gadolinium Break". Angew. Chem. Int. Ed. 56, 13264–13269. https://doi.org/10.1002/anie.201703971.

Wolter, J.-M., Schmeide, K., Weiss, S., Bok, F., Brendler, V., Stumpf, T., 2019. Stability of U(VI) doped calcium silicate hydrate gel in repository-relevant brines studied by leaching experiments and spectroscopy. Chemosphere 218, 241–251. https://doi.org/10.1016/j.chemosphere.2018.11.074.